Exploring the Anticorrosive Efficacy of Drometrizole Derivatives: A DFT, MC and MD Study for Steel Protection

Stanley Numbonui Tasheh[1]*, Rajesh Haldhar[2], Seong-Cheol Kim[2], Narcisse Tsona Tchinda[3], Numbonui Angela Beri[1], Omar Dagdag[4], Avni Berisha[5], Eno Effiong Ebenso[4], Julius Numbonui Ghogomu[1,6]

[1]Department of Chemistry, The University of Bamenda, Bambili-Bamenda, Cameroon
[2]Department of Chemical Engineering, Yeungnam University, Gyeongsan, Republic of Korea
[3]Environment Research Institute, Shandong University, Qingdao, China
[4]Department of Material Science, College of Science, Engineering and Nanotechnology, University of South Africa, Johannesburg, South Africa
[5]Department of Chemistry, University of Prishtina, Tirana, Albania
[6]Department of Chemistry, University of Dschang, Dschang, Cameroon

Research Article

Received: 02-Jan-2025, Manuscript No. JCHEM-25-157571; **Editor assigned:** 07-Jan-2025, PreQC No. JCHEM-25-157571 (PQ); **Reviewed:** 21-Jan-2025, QC No. JCHEM-25-157571; **Revised:** 09-Mar-2025, Manuscript No. JCHEM-25-157571 (R); **Published:** 16-Mar-2025, DOI: 10.4172/2319-9849.14.1.006

***For Correspondence:** Stanley Numbonui Tasheh, Department of Chemistry, The University of Bamenda, Bambili-Bamenda, Cameroon;
E-mail: stanleytash94@gmail.com

Citation: Tasheh SN, et al. Exploring the Anticorrosive Efficacy of Drometrizole Derivatives: A DFT, MC and MD Study for Steel Protection. RRJ Chemist. 2025;14:006.

ABSTRACT

This study investigates the anticorrosive potential of various drometrizole-based organic compounds against mild steel in acidic environments using advanced computational methods, including Density Functional Theory (DFT), Monte Carlo (MC) and Molecular Dynamics (MD) simulations. The focus is on the protonated and non-protonated forms of 2-(2′-hydroxy-5′-methylphenyl)benzotriazole (PBT), along with its derivatives featuring Electron-Donating (ED) and Electron-Withdrawing (EW) groups. Results reveal that both protonated and non-protonated inhibitors can effectively coexist in acidic conditions, demonstrating significant corrosion inhibition for mild steel. The studied compounds exhibit substantial adsorption energies ranging from -3317.1 to -3383.0 kJ/mol for non-protonated species and -3341.9 to -3366.7 kJ/mol for protonated species, aligning parallel to the Fe (110) surface to maximize protective effects. Additionally, pair correlation function values (2.93-3.23 Å for Fe-O and 3.13-3.23 Å for Fe-N interactions) indicate that these inhibitors predominantly engage in physisorption on the Fe (110) surface. Notably, the presence of ED groups markedly enhances the corrosion resistance of PBT derivatives, positioning them as promising candidates for practical applications. This research underscores the need to synthesize ED-based PBT derivatives to develop innovative compounds with superior anti-corrosion properties, paving the way for enhanced protection of steel in challenging environments.

Keywords: Mild steel; Drometrizole; Corrosion inhibitor; DFT; MC simulation; MD simulation

INTRODUCTION

Mild steel due to its outstanding mechanical properties, availability and relatively low cost, is widely regarded as one of the most suitable alloys for industrial applications. Despite these qualities, mild steel is susceptible to corrosion in acidic environments, used for oil well-acidification, pickling, chemical cleaning and acid descaling, leading to substantial economic losses. Consequently, there is an urgent need for the advancement of efficient technologies for corrosion control. In recent times, there has been a greater inclination toward developing organic molecules as corrosion inhibitors owing to the ease with which they are prepared, high inhibition effectiveness at a wide temperature range, compatibility with protected materials, low cost and relatively low toxicity. According to the literature survey, good corrosion inhibitors are organic materials made up of aromatic rings and/or heterocyclic rings consisting of one or more of the heteroatoms O, N, P, and S [1].

Among the organic substances investigated as corrosion inhibitors are: Xanthenes, green inhibitors, surfactants, polymers, imidazoles, Schiff bases, etc. In the ongoing search for efficient organic corrosion inhibitors, less attention has been focused on benzotriazoles such as 2-(2′-hydroxy-5′-methylphenyl)benzotriazole (PBT) also known as Drometrizole or Tinuvin-P (Figure 1), meanwhile, they meet the above-mentioned criteria for good corrosion inhibitors. PBT is a well-known UV absorber and NLO chromophore and can equally serve as a good corrosion inhibitor. Moreover, the presence of some donor and acceptor substituent groups on PBT may enhance its corrosion-inhibitive properties. Unfortunately, both experimental and theoretical studies in this regard are not yet available in the literature to the best of our knowledge. Theoretical and/or experimental studies to explore the potential anti-corrosion properties are necessary as they serve as a great contribution to the ongoing search for excellent organic inhibitors of metal corrosion. In the realm of theoretical chemistry, related mechanistic studies are conveniently carried out using methods such as Density Functional Theory (DFT), Molecular Dynamics (MD) and Monte Carlo (MC) simulations. These methods are more cost-effective and require a lesser time frame than experiments. Indeed, computer simulations have become a powerful tool in the investigation of complex chemical systems for corrosion inhibition. To unravel the anti-corrosion capability of PBT, the main aim of this work was to determine its possible inhibitive mechanisms and potency using the theoretical methods DFT, MD, and MC. PBT has been investigated alongside some of its derivatives encompassing Electron-Donating Groups (EDGs) and Electron-Withdrawing Groups (EWGs), as shown in Figure 1. The effects of the EDGs and EWGs on PBT were investigated to improve upon its anti-corrosion efficiency. Moreover, the protonated counterparts of these molecules were also studied, since these molecules are likely to be protonated in an acidic medium. To attain these goals, MC was used to compute the adsorption energies and to elucidate the interactions between the investigated inhibitors and the Fe (110) surface. MD simulation was used to estimate pair correlation functions (or radial distribution functions) to determine the nature of the inhibitor Fe (110) surface interactions. Furthermore, the conceptual DFT-based global reactivity indices: Electronegativity (χ), absolute softness (σ), absolute hardness (η), back-donation energy ($\Delta E_{B\text{-}D}$), and the fraction of electron transferred (ΔN) have been calculated to predict the anti-corrosion properties of the investigated molecules, as well as electron transfer between the molecules and the metal surface. Finally, local reactivity indices *via* the Hirshfeld population scheme, Frontier Molecular Orbital (FMO) analysis, Natural Population Analysis (NPA), and Molecular Electrostatic Potential (MEP) maps were performed to predict the possible binding and protonation sites of the studied materials [2].

Figure 1. The structure of PBT and its derivatives with an atomic numbering scheme is used in this work. R denotes the Electron-Donating (ED) and Electron-Withdrawing (EW) substituents investigated (note that O16 is the protonation site).

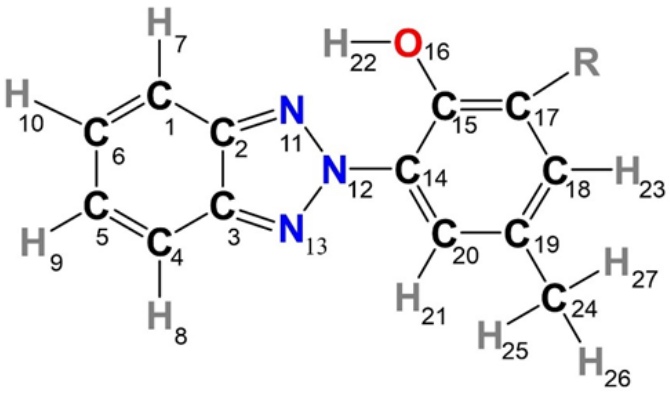

R	Abbreviation	
	Non-protonated	Protonated
-H	PBT	PBTH+
$-NH_2$ (ED)	PBT1	PBT1H+
$-OCH_3$ (ED)	PBT2	PBT2H+
-OH (ED)	PBT3	PBT3H+
-Cl (EW)	PBT4	PBT4H+
-CN (EW)	PBT5	PBT5H+

MATERIALS AND METHODS

Molecular simulation studies

The electronic properties derived from quantum chemical computations by DFT are necessary for the understanding of the mechanism of inhibitors but are inadequate for a detailed description of the metal-inhibitor interactions. Such interactions are better described *via* MC and MD simulations, which are popular techniques for studying metal-inhibitor interactions.

Monte Carlo (MC) simulations: MC simulations were operated to obtain the most stable configurations of the inhibitor-Fe systems with the adsorption energies of different inhibitors on the Fe surface. The interaction between each studied inhibitor and the Fe (110) was explored by the MC simulations utilizing the Material Studio software developed by BIOVIA (formerly Accelrys Inc). The calculations were performed utilizing Condensed-phase Optimized Molecular Potentials for Atomistic Simulation Studies (COMPASS) II (version 1.2) forcefield, in a simulation box with dimensions 17.377 × 17.377 × 10.369 Å with periodic boundary conditions to simulate a representative part of an interface void of any arbitrary boundary effects [3].

Molecular Dynamics (MD) simulation: All MD simulations herein were performed using the Forcite module of the Materials Studio software, in a simulation box (17.377 × 17.377 × 10.369 Å) using periodic boundary conditions. The MD simulation of the behaviour of the inhibitor molecules on the Fe (110) surface was then carried out using the COMPASS II (version 1.2) force field. To simulate a more reliable system, water and hydrogen chloride molecules were added to the solution layer in the simulation box. The liquid phase consisted of 250 H_2O molecules, $5Cl^-$ ions, $5H_3O^+$ ions, and a single dissolved inhibitor molecule. Before the MD simulation, the geometry of the final system was optimized to ensure that its structure was at a local minimum on the potential energy surface.

Quantum chemical calculations

All DFT calculations related to the corrosion inhibitory potentials of the investigated molecules were carried out with the ORCA 4.2.1 computational program suite. Initial guesses for geometry optimization calculations were built with the Avogadro 4.2.1 program. Geometry optimizations of PBT and its derivatives (Figure 1 for atom numbering) in both gas phase, dielectric constant (ε=1.0) and water solvent (ε=78.5) were performed at the B3LYP/def2-TZVP(-f) level of theory. Long-range dispersion interactions were accounted for by the use of the B3LYP functional alongside the atom pairwise dispersion correction based on tight-binding partial charges (D4). Vibrational frequencies were computed at the same level of theory as that used for geometry optimization (B3LYP-D4/def2-TZVP(-f)) and no imaginary frequencies were obtained. This implies that all optimized geometries are stable structures (*i.e.*, minima on the potential energy surface). These computations were carried out employing the grid6 numerical quadrature together with a tight Self-Consistent Field (SCF) convergence criterion.
Water was used as a solvent in these computations to mimic the acid (HCl) environment. Water was chosen here because its dielectric constant is very close to that of dilute HCl (ε=78.3). Moreover, a vast majority of industrial and chemical processes are carried out in an aqueous medium. The solvent effects were accounted for using a universal implicit solvation method known as the Solvation Model Density (SMD) as implemented in ORCA. After full geometry optimization and frequency computations, the energies obtained at the B3LYP-D4/def2-TZVP(-f) level of theory were upgraded *via* Single-Point (SP) calculations at the higher M06-2X/def2-TZVPP level of theory. The frontier molecular orbital energies of the neutral species as achieved from the prior SP estimates were in turn utilized to compute the global reactivity descriptors of the examined molecules [4].
In the acidic medium, the inhibitor molecules are likely to undergo protonation at the heteroatoms (O or N) due to their lone electron pairs. Accordingly, the investigated molecules have been studied along with their protonated counterparts, since these protonated species may also take part in the corrosion inhibition process. To determine the preferred protonation sites, natural (NPA) atomic charge distribution analyses were performed on the optimized non-protonated species. Upon determination of the protonation sites, geometry optimization, frequency, and SP calculations were also carried out on protonated species at the same level of theory as those used for similar calculations on the non-protonated structures. It must be pointed out that all GRDs herein were calculated based on the frontier molecular orbital energies (E_{HOMO} and E_{LUMO}), as follows:

$$\Delta E = E_{LUMO} - E_{HOMO} \quad (1)$$

$$\chi = -\left(\frac{E_{LUMO}+E_{HOMO}}{2}\right) \quad (2)$$

$$\eta = \frac{E_{LUMO}-E_{HOMO}}{2} \quad (3)$$

$$\sigma = \frac{1}{\eta} = \frac{2}{E_{LUMO}-E_{HOMO}} \quad (4)$$

The fraction of electrons transferred (ΔN) between the inhibitor molecules and the atoms of the metallic surface (Fe) was calculated as shown below:

$$\Delta N = \frac{\Phi_{Fe} - \chi_{inh}}{[2(\eta_{Fe} + \eta_{inh})]} \quad (5)$$

where Φ_{Fe} represents the work function of the Fe (1 1 0) plane with a value of 4.82 eV mol^{-1}, χ_{inh} is the electronegativity of the inhibitor molecule, η_{Fe} (0 eV mol^{-1}) and η_{inh} are the absolute hardness of Fe (110) and the inhibitor molecules, respectively.

The energy arising from the back-donation of charges was calculated as follows:

$$\Delta E_{B-D} = -\frac{\eta}{4} \quad (6)$$

RESULTS AND DISCUSSION

Atomistic simulation results

The results obtained from Monte Carlo and molecular dynamics simulations are reported and discussed herein.

Monte Carlo simulation results: Monte Carlo (MC) simulation is an appropriate tool for investigating the most stable configuration of the molecule susceptible to adsorption on metal surfaces. It involves the search for low-energy adsorption sites on both periodic and non-periodic substrates. The equilibrium configurations (top and side view) of the non-protonated and protonated forms of the inhibitors adsorbed on the Fe (110) surface. Several outputs and descriptors of the MC simulation are presented in Tables 1 and 2 for the non-protonated and protonated species respectively [5].

Table 1. Descriptors calculated from MC simulations for the non-protonated molecules/Fe (110)/250 H_2O/5Cl^-/5H_3O^+ system (in kCalmol^{-1}).

	PBT	PBT1	PBT2	PBT3	PBT4	PBT5
Total energy	-3324.68	-3248.26	-3266.19	-3296.54	-3294.63	-3274.72
Adsorption energy	-3366.67	-3341.92	-3348.63	-3357.71	-3346.28	-3349.98
Rigid adsorption energy	-3441.76	-3388.89	-3425.54	-3434.72	-3423.38	-3390.1
Deformation energy	75.08	46.97	76.92	77.01	77.1	40.12
Compound dE_{ad}/dNi	-181.61	-134.29	-141.17	-167.46	-146.74	-130.16
H_2O dE_{ad}/dNi	-12.02	-11.34	-11.51	-11.21	-10.01	-10.8
H_3O^+ dE_{ad}/dNi	-159.87	-162.76	-156.81	-164.15	-158.88	-151.83
Cl^- dE_{ad}/dNi	-145.23	-147.9	-147.68	-144.37	-148.75	-148.83

The parameters presented in the tables encompass: The energy of substrate–adsorbate configurations (dE_{ads}/dNi), the total

energy of the substrate-adsorbate configuration, and the rigid adsorption energy and the deformation energy. The rigid adsorption energy, the deformation energy and the energies of the adsorbate components are added to create the overall energy. Here, it is assumed that the substrate energy (Fe (110) surface) is zero. Additionally, the adsorption energy is the amount of energy released or needed to bind the relaxed adsorbate components. The rigid adsorption energy as well as the deformation energy for the components of the adsorbate make up the adsorption energy. The energy generated or needed when the complicated environment adsorbate components are adsorbed on the surface is represented by the rigid adsorption energy. The energy generated when the deposited adsorbate components are loosened on the substrate surface is reported as the deformation energy. Additionally, these tables display (dE_{ads}/dNi), which represents the energy of substrate-adsorbate combinations in which one of the adsorbate elements has been eliminated [6].

Table 2. Descriptors calculated from MC simulations for the protonated molecules/Fe (110)/250 H_2O/5Cl^-/5H_3O^+ system (in kCalmol^{-1}).

	PBTH$^+$	PBTH1$^+$	PBTH2$^+$	PBTH3$^+$	PBTH4$^+$	PBTH5$^+$
Total energy	-3348.26	-3335.36	-3341.53	-3359.42	-3334.94	-3277.34
Adsorption energy	-3349.12	-3338.95	-3380.73	-3383	-3366.87	-3317.06
Rigid adsorption energy	-3446.73	-3436.7	-3455.96	-3456.58	-3440.81	-3393.56
Deformation energy	97.61	97.76	75.23	73.58	73.93	76.5
Compound dE_{ad}/dNi	-164.3	-165.25	-201.23	-187.45	-190.3	-111.63
H_2O dE_{ad}/dNi	-11.73	-11.38	-11.24	-10.51	-11.27	-10.96
H_3O^+ dE_{ad}/dNi	-160.62	-158.46	-152.62	-155.92	-161	-145.97
Cl^- dE_{ad}/dNi	-148.6	-143.88	-150.23	-141.76	-148.37	-154.64

For all the molecules studied, the adsorption energies of the inhibitors are by far greater than those of water molecules (Tables 1 and 2). This illustrates the possibility of a slow replacement of water molecules from the Fe surface resulting in the formation of a stable layer that protects the surface from aqueous corrosion.

All the inhibitors are found to be planar and therefore are capable of being adsorbed on the Fe (110) surface in a parallel manner, thereby maximizing surface contact and enhancing surface coverage of the metal. Conclusively, MC simulations reveal the molecules studied lie in a parallel manner on the Fe (110) surface and possess very high adsorption energies, implying they are adsorbed strongly and spontaneously on the Fe (110) surfaces.

Molecular dynamics simulation results: Molecular Dynamics (MD) simulations were performed here to examine the inhibitor-Fe (110) surface interaction type *via* the pair correlation function or Radial Distribution Function (RDF). RDFs are commonly used as a convenient method to investigate the inhibitor-metal bond length [7].

The interaction of the studied molecules with the surface of the metal depends mainly on the nature of the bonds established between the atoms of these molecules and the Fe-atoms present on the metal surface. According to the literature, chemisorption is established within a bond length range of 1–3.5 Å, whereas physisorption is greater than 3.5 Å. Due to the major role heteroatoms (such as O and N) play in the adsorption process, only the distances of the Fe-O (g_{Fe-O}) and Fe-N (g_{Fe-N}) bonds between the investigated substrates and the metal surface were considered in this study, and their values are presented in Table 3. The results indicate that the bond lengths range from 2.99-3.23 for g_{Fe-O} and from 3.13-3.23 for g_{Fe-N} for the non-protonated molecules. Similarly, the RDF values of the protonated species range from 2.93-3.09 Å for g_{Fe-O} and from 3.15-3.19 Å for g_{Fe-N}. From Table 3, the RDF values are lower than 3.5 Å but greater than 2 Å, suggesting that the adsorption type between the inhibitors and the Fe (110) surface is predominantly physisorption. Further insight in this regard can be obtained by using a reactive force field.

Table 3. RDFs (in Å) of the non-protonated and protonated systems at 298 K.

Non-protonated						
RDF	PBT	PBT1	PBT2	PBT3	PBT4	PBT5
g_{Fe-N}	3.15	3.23	3.17	3.15	3.13	3.13

g_{Fe-O}	3.09	3.17	3.13	2.99	3.03	3.23
Protonated						
RDF	$PBTH^+$	$PBT1H^+$	$PBT2H^+$	$PBT3H^+$	$PBT4H^+$	$PBT5H^+$
g_{Fe-N}	3.15	3.19	3.17	3.17	3.17	3.15
g_{Fe-O}	3.01	3.07	2.93	3.09	3.07	3.03

RDF analyses confirm the inhibitors' strong tendencies to donate and receive electrons from the metal surface thereby adsorbing and protecting the metal.

Mechanism of corrosion inhibition

Based on the theoretical results, a plausible inhibition mechanism of the investigated inhibitor molecules of mild steel corrosion in the acidic medium can be proposed as follows:

- The non-protonated inhibitors (PBT, PBT1, PBT2, PBT3, PBT4, and PBT5) can be adsorbed on the steel surface *via* the chemisorption mechanism and *via* coordinate bonds that are formed between lone electron pairs of the non-protonated O or N atoms and the empty d-orbital of Fe atoms.
- PBT1, PBT2, PBT3, PBT4, and PBT5 can also be adsorbed on the metal surface based on donor-acceptor interactions between π-electrons of the benzotriazole and 4-methoxy phenolic rings and vacant d-orbitals of Fe.
- The non-protonated O atoms in PBT, PBT1, PBT2, PBT3, PBT4, and PBT5 can be protonated in the acid solution which can then be adsorbed on the cationic steel surface already saturated by negative Cl^- ions from the acid.

Protonated forms of benzotriazole molecules compete for aqueous H^+, yet upon the arrival of H_2 gas, the molecule returns to the unprotected structure. When heteroatoms in molecules return to non-protonated forms, the transfer of unshared electron pairs into the unoccupied d-orbital of the metal follows.
The suggested mechanism of adsorption of PBT and derivatives is shown in Figure 2.

Figure 2. Schematic representation of the surface adsorption mechanism of the inhibitor molecules on the mild steel surface in aqueous media.

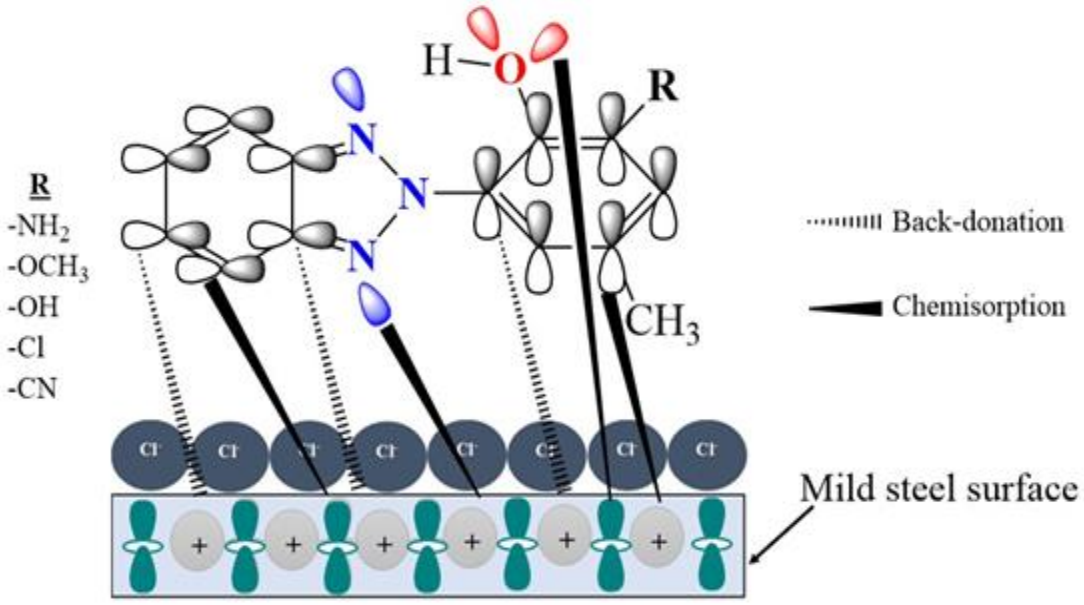

These outcomes have been completely approved with impedance studies, showing that the inhibitory impact is brought about by the mixture of π-electrons and heteroatoms that assume a key part in various inhibitor molecules to donate or accept the electron from the Fe (110) surface [8].

Assessing the suitability of the optimized structures

To ascertain the suitability of the B3LYP-D4/def2-TZVP(-f) level of theory, and the precision of the optimized structures, selected gas-phase computed bond lengths and angles of PBT have been compared with the corresponding experimental values. The calculated bond lengths are listed in Table 4, along with the corresponding experimental values [9].

Table 4. Selected gas-phase computed bond lengths and angles of PBT at the B3LYP-D4/def2-TZVP(-f) level of theory.

	Bond lengths[a] (Å)			Bond angles[a] (°)	
Bond type	Expt[b].	Compt[c].	Bond type	Expt[b].	Compt[c].
C1-C2	1.407	1.406	C2-C3-C4	121.1	121
C2-C3	1.402	1.418	C6-C1-C2	116.1	116.7
C3-C4	1.404	1.407	C4-C5-C6	121.8	121.9
C4-C5	1.361	1.373	C5-C6-C1	122.8	122
C5-C6	1.409	1.421	C5-C4-C3	116.8	116.9
C6-C1	1.358	1.373	C2-C3-N13	109.2	108.6
C2-N11	1.349	1.345	N13-C3-C2	109.2	108.6
C3-N13	1.352	1.347	N12-N13-C3	102.8	103.6
N11-N12	1.34	1.336	N12-N11-C2	103.2	103.9
N12-N13	1.33	1.322	N12-C14-C15	120.5	120.7
N12-C14	1.43	1.42	C14-C15-O16	124.6	124.5
C14-C15	1.398	1.406	C15-C17-C18	121	121.1
C14-C20	1.385	1.396	C17-C18-C19	121.7	121.4
C15-O16	1.361	1.346	C18-C19-C20	116.9	117.8
C15-C17	1.383	1.396	C19-C20-C14	122.3	121.3
C17-C18	1.379	1.38	C20-C14-C15	120.1	120.7
C18-C19	1.392	1.4	C18-C19-C25	121.2	121
C19-C20	1.38	1.384			
C19-C25	1.499	1.507			

Note: [a]Refer to Figure 1 for atomic numbering
[b]Experimental values of selected bond lengths and angles obtained from
[c]Computed values of selected bond lengths and angles from this work at the B3LYP-D4/def2-TZVP(-f) level of theory

The outcomes show that the theoretical bond angles and bond lengths are in good agreement with experimental data demonstrating the suitability of the technique utilized. For a clearer comparison of these examination results, simple linear regression was accomplished to get the correlation coefficients (R^2) of 0.9329 and 0.9942, respectively. The R^2 values are exceptionally near unity, implying that the estimation of the computed bond angle and bond length of these studied inhibitor molecules were steady with the experimental results. This shows the reliability of optimized structures herein.

Geometrical analyses of the protonated and non-protonated species in the aqueous phase

Inhibitor molecules with highly planar geometries are usually easily adsorbed and consequently possess high inhibition capabilities on metal surfaces. From this perspective, it was vital to analyse the structural parameters, particularly the bond and dihedral angles, of the investigated inhibitor molecules in a bid to determine their planarity. The fully optimized structures of the non-protonated species denoted: PBT, PBT1, PBT2, PBT3, PBT4 and PBT5, and the protonated species: $PBTH^+$, $PBT1H^+$, $PBT2H^+$, $PBT3H^+$, $PBT4H^+$ and $PBT5H^+$, obtained at the B3LYP-D4/def2-TZVP(-f) in the aqueous phase are displayed in Figures 3 and 4 as visualized using the ChemCraft v1.7 software. Some selected geometric parameters of these molecules are listed in Table 5.

Table 5. Selected geometric parameters of PBT and its derivatives optimized at the B3LYP-D4/def2-TZVP(-f) in the aqueous phase.

Non-protonated						
Parameters	**PBT**	**PBT1**	**PBT2**	**PBT3**	**PBT4**	**PBT5**
Bond angles[a] (°)						
N11-N12-C14	121.4	121.1	121.3	116.1	121.1	121.2
C15-C14-N12	120.8	119.6	120	119.9	119.7	120.1
C15-C17-C18	121	119	120.6	121.1	122.3	121.5
O16-C15-C17	117.8	116.9	117.4	117.4	119.3	118.1
Dihedral angles[a] (°)						
O16-C15-C14-C20	-178.2	179.5	-179.1	-179.2	-179.2	-178.3
O16-C15-C17-C18	178.8	-178.8	179.1	179.2	179.5	178.4
Protonated						
	$PBTH^+$	**$PBT1H^+$**	**$PBT2H^+$**	**$PBT3H^+$**	**$PBT4H^+$**	**$PBT5H^+$**
Bond angles[a] (°)						
N11-N12-C14	123.5	123.5	123.6	123.2	112.5	112.4
C15-C14-N12	121.3	121.3	120.7	120.4	120.4	117.5
C15-C17-C18	120.6	120.6	120.5	120.8	122.1	121
O16-C15-C17	121.9	121.9	120	120.3	122.9	123.1
Dihedral angles[a] (°)						
O16-C15-C14-C20	-178	-178.1	-179	-179.2	-179	179.7
O16-C15-C17-C18	178.5	178.6	179.2	179.5	179.3	-179.5
Note: [a]Refer to Figures 3 and 4 for atomic numbering						

It is worthy of note that the parameters listed in Table 5 are selected from the 4-methoxy phenolic ring, since changes caused by the EDGs and EWGs at atom C17 of this ring, or changes arising from protonation, may result in some loss of planarity of PBT or $PBTH^+$. The results indicate that for every investigated molecule to be perfectly planar, the bond angles listed in Table 5 should each be close to 120o. It turns out that the values of these angles (116.9–122.3° and 112.5–123.5° for the non-protonated and protonated geometries, respectively) deviate slightly from 120°. It is certain from the bond angles that the non-protonated molecules are more planar than the protonated ones. The results also show that the absolute values of the torsional angles in the 4-methoxy phenolic ring are very close to 180° for both the protonated and non-protonated species. Also, the nature of the substitution (*i.e.,* of EDGs or EWGs) on C17 of the 4-methoxy phenolic ring, and the protonation on atom O16 has not got an appreciable effect on the selected geometrical parameters.

Figure 3. Optimized geometric structures of the neutral inhibitors computed at the B3LYP-D4/def2-TZVP(-f) level of theory in the aqueous phase.

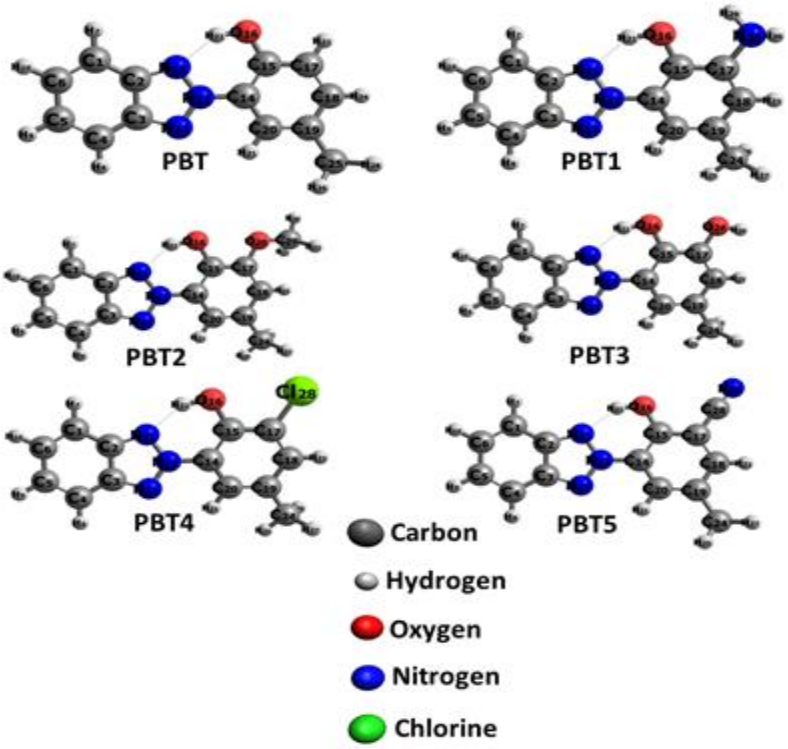

Figure 4. Optimized geometric structures of the neutral inhibitors computed at the B3LYP-D4/def2-TZVP(-f) level of theory in the aqueous phase.

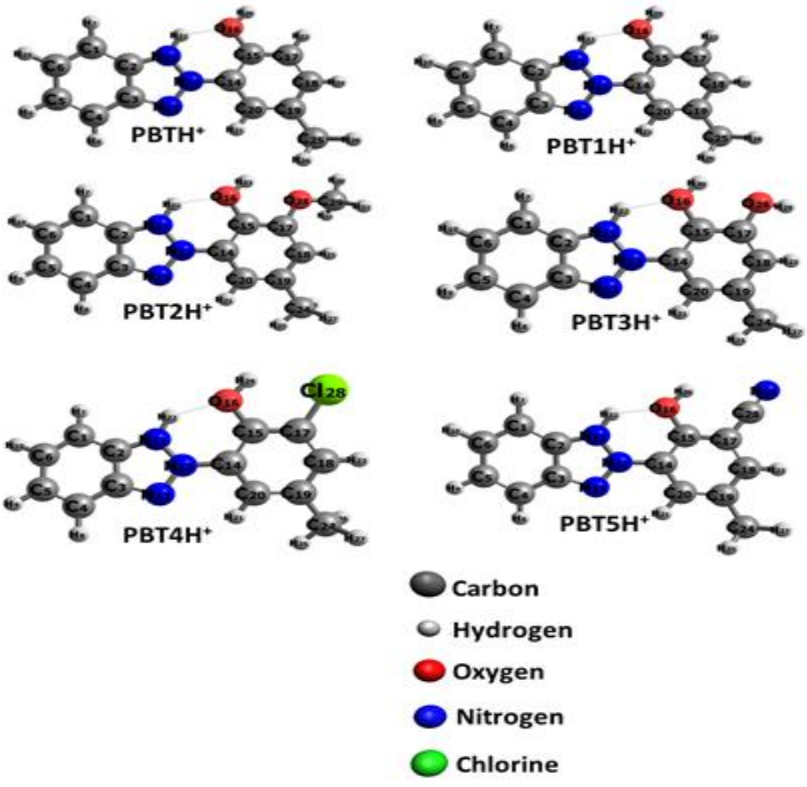

Based on the foregoing, it can be concluded that the optimized molecular structures of the investigated molecules are highly planar and are thus expected to be readily adsorbed and have high inhibition capabilities on the Fe-surface.

Conceptual-DFT-based prediction of inhibitory potentials of the protonated and non-protonated molecules in the aqueous phase

The Global Reactivity Descriptors (GRDs) of the molecules studied, as E_{HOMO}, E_{LUMO}, ΔE, η, σ, χ, ΔN, and $\Delta E_{B\text{-}D}$ have been used to elucidate the electron transfer mechanisms between the inhibitor molecules and mild steel surfaces. The computed C-DFT-based parameters of the non-protonated and protonated forms of the molecules together with those of benzotriazole (BTAH) in the aqueous phase are given in Table 6. The graphical variations of the HOMO energy. HOMO-LUMO energy gap, hardness, softness, electronegativity, fractions of electrons transferred, and the back-donation energy concerning the non-protonated and protonated species in the aqueous phase respectively are provided of the accompanying Electronic Supplementary Material (ESM).

Table 6. Calculated quantum chemical parameters (in eV) of the non-protonated and protonated inhibitors at the M06-2x/D3Zero/def2-TZVPP level of theory in the aqueous phase.

Non-protonated								
Species	**E_{HOMO}**	**E_{LUMO}**	**$\Delta E_{H\text{-}L}$**	**η**	**σ^a**	**χ**	**ΔN**	**$\Delta E_{B\text{-}D}$**
PBT5	-7.7416	-1.5255	6.2161	3.1081	0.3217	4.6336	0.03	-0.777
PBT4	-7.6333	-1.408	6.2253	3.1127	0.3213	4.5207	0.0481	-0.7782
PBT	-7.4747	-1.3263	6.1484	3.0742	0.3253	4.4005	0.0682	-0.7686
PBT3	-7.4293	-1.3332	6.0961	3.0481	0.3281	4.3813	0.072	-0.762
PBT2	-7.3637	-1.3162	6.0475	3.0238	0.3307	4.34	0.0794	-0.7559
PBT1	-7.1067	-1.238	5.8687	2.9344	0.3408	4.1724	0.1104	-0.7336
BTAH	-8.068	-0.4834	7.5846	3.7923	0.2637	4.2757	0.0718	-0.9481
Protonated								
Species	**E_{HOMO}**	**E_{LUMO}**	**$\Delta E_{H\text{-}L}$**	**η**	**σ^a**	**χ**	**ΔN**	**$\Delta E_{B\text{-}D}$**
$PBT5H^+$	-8.2667	-2.2719	5.9948	2.9974	0.3336	5.2693	-0.0749	-0.7494
$PBT4H^+$	-8.1664	-2.2082	5.9582	2.9791	0.3357	5.1873	-0.0616	-0.7448
$PBTH^+$	-7.9645	-2.1172	5.8473	2.9237	0.342	5.0409	-0.0378	-0.7309
$PBT3H^+$	-7.8687	-2.1331	5.7356	2.8678	0.3487	5.0009	-0.0315	-0.717
$PBT2H^+$	-7.7864	-2.123	5.6634	2.8317	0.3531	4.9547	-0.0238	-0.7079
$PBT1H^+$	-7.4988	-2.1073	5.3915	2.6958	0.371	4.8031	0.0031	-0.6739
$BTAH^+$	-8.726	-1.7517	6.9743	3.4872	0.2868	5.2389	-0.0601	-0.8718
Note: σ^a Softness values in eV^{-1}								

Highest occupied molecular energy: FMO energies (*i.e.,* E_{HOMO} and E_{LUMO}), which are dependent on the frontier molecular orbital and the fukui theories, are significant in forecasting the chemical reactivity and stability of molecules. E_{HOMO} often refers to a molecule's capacity to donate electrons. The likelihood of a molecule donating electrons to suitable acceptors increases with increasing E_{HOMO} value. The findings indicate how both species of the molecules under study had larger E_{HOMO} values than those of BTAH, indicating a stronger propensity for electron emission. The outcomes also show that the non-protonated molecules had E_{HOMO} values that are around 0.5 eV greater than their protonated counterparts. This implies that the non-protonated inhibitors have a greater ability to donate electrons to the vacant 3d orbital of Fe than the protonated ones. This also suggests that protonation reduces the electron-donation ability of the inhibitors studied. This is expected because the protonation of a molecule results in an increased nuclear charge which attracts the outer electrons more strongly, thus increasing the Ionization Potential (IP) of the protonated species relative to that of the non-protonated species. Accordingly, the inhibition efficiency of the studied inhibitors increases in the order:

$E_{HOMO_{BTAH}} < E_{HOMO_{PBT5}} < E_{HOMO_{PBT4}} < E_{HOMO_{PBT}} < E_{HOMO_{PBT3}} < E_{HOMO_{PBT2}} < E_{HOMO_{PBT1}}$ for the non-protonated species and in the order: $E_{HOMO_{BTAH^+}} < E_{HOMO_{PBT5H^+}} < E_{HOMO_{PBT4H^+}} < E_{HOMO_{PBTH^+}} < E_{HOMO_{PBT3H^+}} < E_{HOMO_{PBT2H^+}} < E_{HOMO_{PBT1H^+}}$ for the protonated species in the aqueous phase.

Highest occupied molecular orbital energy-Lowest unoccupied molecular orbital energy gap: The HOMO-LUMO energy gap (ΔE) is known to provide useful information on the reactivity and stability of molecules. Typically, a molecule's reactivity varies inversely with its ΔE. Consequently, molecules with low ΔE values are more polarizable and are generally associated with high chemical reactivity, low kinetic stability, and consequently easy electron transfer. The results indicate that the ΔE values of the molecules studied are about 1.5 times lower than those of BTAH. This implies that the transfer of electrons from the molecules studied to the surface of iron is easier in the PBT and derivatives than in BTAH, making them more polarizable. The results also show that the ΔE values of the protonated molecules are lower than those of the non-protonated molecules by approximately 0.3 eV (Table 6). Therefore, protonation reduces ΔE values. This means that the protonated species are the most reactive form of each inhibitor. Again, the results portray that molecules with EDGs have lower ΔE values, while those with EWGs have relatively higher ΔE values, as compared with the ΔE values of the unsubstituted molecules (PBT and PBT1H⁺). The presence of EDGs is found to reduce the ΔE values by about 0.1 and 0.3 eV for the non-protonated and the protonated molecules respectively. Based on the ΔE values of the inhibitors, the order of increasing inhibition is:

$\Delta E_{BTAH} < \Delta E_{PBT4} < \Delta E_{PBT5} < \Delta E_{PBT} < \Delta E_{PBT3} < \Delta E_{PBT2} < \Delta E_{PBT1}$ for the non-protonated species, and: $\Delta E_{BTAH^+} < \Delta E_{PBT5H^+} < \Delta E_{PBT4H^+} < \Delta E_{PBTH^+} < \Delta E_{PBT3H^+} < \Delta E_{PBT2H^+} < \Delta E_{PBT1H^+}$ for the protonated species in the aqueous phase. Trends are consistent with those obtained from the E_{HOMO} values.

Global softness: Global softness (σ) is also an important quantum parameter that is commonly used to explain chemical reactivity. It has been established that greater adsorption of an inhibitor on a metal surface occurs at the molecular site where is highest. The results depict that the σ values of the PBT and derivatives for both species are about 0.06 times lower than those of BTAH. It also shows that the σ values of the protonated compounds are slightly higher than those of the non-protonated ones by about 0.02 eV (Table 6). It implies that protonation increases the σ values of the molecules studied. This illustrates that the protonated species are slightly more polarizable and kinetically more stable than the non-protonated counterparts.

The findings also indicate that the inhibitors containing EDGs have the highest σ values, while those with the EWGs have the lowest σ values. Accordingly, the corrosion inhibition efficiency of the molecules studied based on the χ values increases in the order:

$\sigma_{BTAH} < \sigma_{PBT4} < \sigma_{PBT5} < \sigma_{PBT} < \sigma_{PBT3} < \sigma_{PBT2} < \sigma_{PBT1}$ for the non-protonated species and in the order: $\sigma_{BTAH^+} < \sigma_{PBT5H^+} < \sigma_{PBT4H^+} < \sigma_{PBTH^+} < \sigma_{PBT3H^+} < \sigma_{PBT2H^+} < \sigma_{PBT1H^+}$ for the protonated species in water. These trends are in perfect agreement with those derived from the ΔE values.

Electronegativity: Electronegativity (χ) describes a molecule's ability to attract electrons. Molecules with lower χ are expected to have high inhibition efficiency because they are likely to donate electrons to the metal surface. The outcome points out that the χ values of the non-protonated species are lower than those of the protonated ones in water solvent by at least 0.7 eV. This implies that protonation increases the electronegativity of the molecules under investigation. Consequently, the non-protonated molecules have a lower affinity for electrons and may therefore attract fewer electrons from the 3d-orbitals of Fe. Also, the presence of EDGs leads to a reduction of χ, while that of EWGs acts otherwise.

Based on the χ values, the corrosion inhibitive capacity of the molecules studied increases in the order:

$\chi_{PBT5} < \chi_{PBT4} < \chi_{PBT} < \chi_{PBT3} < \chi_{PBT2} < \chi_{BTAH} < \chi_{PBT1}$ for the non-protonated species in the water solvent, and in the order: $\chi_{PBT5H^+} < \chi_{BTAH^+} < \chi_{PBT4H^+} < \chi_{PBTH^+} < \chi_{PBT3H^+} < \chi_{PBT2H^+} < \chi_{PBT1H^+}$ for the protonated counterparts in the water solvent.

Fractions of electrons transferred: The fraction of electrons transferred (ΔN) is another important indicator of a molecule's propensity to donate electrons to the atoms of metal to adhere firmly to its surface. Generally, molecules with high electron transfer tendencies are considered to have very high abilities to interact with metal surfaces, and vice-versa. If ΔN>0, electron transfer occurs from the inhibitor molecule to the metal surface, whereas if ΔN<0, the transfer is otherwise. The results show that the ΔN values for the non-protonated forms of the inhibitors are positive (*i.e.,* ΔN>0), but become negative (*i.e.,* ΔN<0) upon protonation except for PBT1H⁺. Accordingly, the non-protonated inhibitors are expected to act as electron donors, while the protonated ones as electron acceptors during the Inhibitor-Fe interactions. Consequently, the non-protonated species are capable of binding more tightly to the surface of mild steel, thereby forming a corrosion-inhibitive adsorption layer than the protonated ones. To add, ΔN for both investigated species is less 3.6. This agrees with Lukovit's findings whereby the inhibitive efficacy increases with increasing electron-donating ability to a metal surface.
Furthermore, the presence of EDGs increases ΔN, while the presence of EWGs, decreases ΔN. It is interesting to note that both χ and ΔN have revealed the same corrosion inhibitive trends for the molecules investigated, which are:

$\Delta N_{PBT5} < \Delta N_{PBT4} < \Delta N_{PBT} < \Delta N_{BTAH} < \Delta N_{PBT3} < \Delta N_{PBT2} < \Delta N_{PBT1}$ for the non-protonated species and $\Delta N_{PBT5H+} < \Delta N_{PBT4H+} < \Delta N_{BTAH+} < \Delta N_{PBTH+} < \Delta N_{PBT3H+} < \Delta N_{PBT2H+} < \Delta N_{PBT1H+}$ for the protonated species.

Hardness: Hardness (η) is a measure of a molecule's resistance to electron cloud polarization or deformation under little perturbations of a chemical reaction. Molecules with high are very stable and are not efficient corrosion inhibitors, while those with low are unstable and can readily react with the metal surface, thus they are efficient corrosion inhibitors. Owing to the reluctance to give out electrons, η varies inversely with inhibition efficiency. The η values of PBT and derivatives are found to be approximately 0.7 times lower than those of BTAH. In addition, the η values of the protonated molecules are lower than those of the non-protonated ones. Also, the inhibitor molecules with EDGs have lower η values than those with EWGs. Based on chemical hardness, the protonated molecules are better corrosion inhibitors than the non-protonated ones, and the inhibitors bearing EDGs have greater inhibitive potentials than those bearing EWGs.
Back-donation energy: According to the simple charge transfer model proposed by Gomez and collaborators, the donation and back-donation of electrons govern inhibitor-metal interactions. The $\Delta E_{B\text{-}D}$ values of the protonated molecules are found to be larger than those of the non-protonated counterparts. This means that the protonated molecules can more readily accept back-donated electrons from the metal surface than the non-protonated ones. Table 6 also shows that the presence of EDGs increases the ability to accept back-donated electrons, while that of EWGs reduces this ability.
The results in Table 6 indicate that η>0 and $\Delta E_{B\text{-}D}$<0 for both the protonated and non-protonated forms of the studied molecules. This is suggestive of the fact that electron transfer from the molecules to the metal surface can be followed by the back-donation of electrons from the metal to the molecules. It is also clear from the negative values of $\Delta E_{B\text{-}D}$ that back-donation is energetically favoured. It follows from the values of η and $\Delta E_{B\text{-}D}$ that the inhibition efficiency of the currently investigated inhibitors increases in the order: BTAH<PBT4<PBT5<PBT<PBT3<PBT2<PBT1 for the non-protonated species, and in the order: $BTAH^+<PBT4H^+<PBT5H^+<PBTH^+<PBT3H^+<PBT2H^+<PBT1H^+$ for the protonated species. Once again, these trends are in perfect agreement with those derived from the E_{HOMO}, ΔE, σ, χ, and ΔN values.
Among the GRDs discussed above, ΔE, σ, η and $\Delta E_{B\text{-}D}$ reveal the high corrosion inhibition capacity of the protonated molecules, while E_{HOMO}, χ, and ΔN have indicated high corrosion inhibition potentials of the non-protonated molecules. This leads to the conclusion that both the protonated and the non-protonated forms of the investigated molecules are efficient corrosion inhibitors for mild steel in the aqueous acidic medium. It is obvious from these GRDs that significant improvements in corrosion inhibition are acquired by appending EDGs onto PBT and $PBTH^+$. Interestingly, the greatest improvement in corrosion inhibition efficacy arises when the $-NH_2$ group is attached to the C17 carbon atom of the 4-methoxy phenolic moiety in both PBT and $PBTH^+$. This is following the well-established fact that electron-donating substituents like $-NH_2$, $-OCH_3$ and –OH increase electron density on inhibitor molecules thereby facilitating the donor-

acceptor interactions between such molecules and mild steel, which enhances the corrosion inhibition efficiency of the molecules.

Determination of inhibitor-based metal-binding sites

Inhibitor molecules can bind to metal surfaces *via* electron transfer (either by donating or accepting electrons). It is therefore imperative to identify the possible metal-binding sites in the molecules under investigation. To this end, three electronic properties were investigated, namely: the partial atomic charge, the Fukui function indices, and Molecular Electrostatic Potential (MEP) maps.

Partial atomic charges: Atomic charge distribution can facilitate the identification of the most probable binding sites of the inhibitor molecules to the surface of mild steel. Atoms with the most negative partial charges have the highest tendency to donate electrons, thereby getting absorbed onto the metal surface. The studied molecules are likely to interact with the surface of Fe through such atoms. To determine such atomic binding sites, net atomic charges were computed herein within the framework of the Natural Population Analysis (NPA) scheme, and the values are listed in Table 7 for the non-protonated and protonated molecules in the aqueous phase and compared graphically. For the sake of clarity, only the natural charges on the heteroatoms are shown. It is important to note that these charges were calculated with the aid of the JANPA program using ORCA-generated input files at the M06-2X D3Zero/def2-TZVPP level of theory in the aqueous phase.

Table 7. JANPA-based natural population analysis charges of the non-protonated and protonated molecules in the aqueous phase computed at the M06-2x/D3Zero/def2-TZVPP level.

Non-protonated						
Atoms	**PBTH**	**PBT1**	**PBT2**	**PBT3**	**PBT4**	**PBT5**
N11	-0.299	-0.299	-0.299	-0.299	-0.297	-0.296
N12	0.072	0.069	0.072	0.071	0.069	0.069
N13	-0.244	-0.24	-0.241	-0.241	-0.237	-0.236
O16	-0.705	-0.714	-0.699	-0.701	-0.692	-0.684
Protonated						
Atoms	**PBTH$^+$**	**PBT1H$^+$**	**PBT2H$^+$**	**PBT3H$^+$**	**PBT4H$^+$**	**PBT5H$^+$**
N11	-0.264	-0.264	-0.264	-0.264	-0.26	-0.26
N12	0.126	0.125	0.121	0.124	0.121	0.12
N13	-0.15	-0.147	-0.146	-0.146	-0.14	-0.142
O16	-0.696	-0.691	-0.723	-0.692	-0.68	-0.672

Our findings depict those atoms: O16, N11, and N13 are the most probable reactive sites for interaction with the Fe surface since they possess relatively larger negative charges. These atoms are ranked as follows according to the decreasing magnitudes of their negative charges: O16>N13>N11. The results also show that all the heteroatoms (except N12) have high negative charge densities, implying that the most probable reactive site for the adsorption of these inhibitors on mild steel surfaces is centred on these atoms. It is noteworthy that atom N12 which carries positive charges is the site in which the molecules could accept electrons from the unoccupied 3d-orbital of the metal. Interestingly, for the individual molecules (both non-protonated and protonated), the highest negative atomic charge is on atom O16 since Oxygen has two more electrons compared to nitrogen, making it more reactive. This atom is considered the preferred site for giving out electrons to the surface of mild steel to form a dative covalent bond. Atom O16 is, therefore, more likely to partake in an electrophilic attack, whereby it will easily give electrons to the electrophilic species. The NPA results conform with the RDF predictions which show that the O-atom is the most probable binding site to the Fe (110) surface.

CONCLUSION

2-(2′-hydroxy-5′-methylphenyl)benzotriazole (PBT) is a highly studied UV absorber, which may also function as an anti-corrosion agent, but its corrosion inhibitory properties are less investigated. To bridge this gap, this work was aimed at investigating the anticorrosion efficiency of drometrizole for mild steel in acid media. Furthermore, the effects of ED and EW

groups, as well as the influence of protonation, on the corrosion efficiency of drometrizole were studied herein *via* DFT, MD, and MC computations. Highly negative adsorption energies, obtained herein *via* MC simulations, are indicative of the spontaneity of absorption of the investigated molecules on the surface of Fe (110). It has been found from MC simulation snapshots that the inhibitors are planar and parallel to the Fe (110) surface, which provides maximum contact with the surface, thereby maximizing the protection of the metal from corrosion. RDF values for both the protonated and non-protonated molecules as obtained from MD simulation are less than 3.5 Å but greater than 2 Å, indicating that the inhibitors are predominantly physisorbed on the Fe (110) surface. DFT results have identified drometrizole as a potential corrosion inhibitor. Moreover, the presence of the ED groups, as opposed to the EW groups, is found to greatly increase the anti-corrosive potentials of PBT. The results have also shown that both the protonated and non-protonated species can co-exist in the acid medium, which is quite beneficial for the corrosion of mild steel in acid media. According to local reactivity analysis *via* the NPA scheme, the lone O atom of PBT is the most susceptible binding site to electrophilic attack. According to our results, drometrizole and its derivatives are effective inhibitors of mild steel corrosion in acid media. Based on these results, the molecules under investigation are potential inhibitors of mild steel corrosion in acid media during industrial processes like cleaning, pickling, and oil-well acidification.

DATA AVAILABILITY STATEMENT

The data supporting the findings of this study are available upon reasonable request.

CONFLICTS OF INTsEREST

The authors declare no conflicts of interest.

FUNDING

No funding was received.

ACKNOWLEDGEMENT

The authors acknowledge the annual research modernization grant to lecturers by the Ministry of Higher Education of Cameroon.

REFERENCES

1. Fitoz A, et al. An experimental and theoretical approach towards understanding the inhibitive behavior of a nitrile substituted coumarin compound as an effective acidic media inhibitor. Corr Sci. 2018;133:451-464.
2. Benhiba F, et al. Nitro substituent effect on the electronic behavior and inhibitory performance of two quinoxaline derivatives in relation to the corrosion of mild steel in 1M HCl. J Mol Liq. 2020;312:113367.
3. Chugh B, et al. Comparative investigation of corrosion-mitigating behavior of thiadiazole-derived bis-schiff bases for mild steel in acid medium: Experimental, theoretical, and surface study. ACS Omega. 2020;5:13503-13520.
4. Mahdi BS, et al. Corrosion inhibition of mild steel in hydrochloric acid environment using terephthaldehyde based on Schiff base: Gravimetric, thermodynamic, and computational studies. Molecules. 2022;27:4857.
5. Galai M, et al. α-Brass and (α+β) brass degradation processes in azrou soil medium used in plumbing devices. J Bio Tribo Corros. 2017;3:30.
6. Kadiri L, et al. *Coriandrum sativum*. L seeds extract as a novel green corrosion inhibitor for mild steel in 1.0 M hydrochloric and 0.5 M sulfuric solutions. Anal Bioanal Electrochem. 2018;10:249-268.
7. Errahmany N, et al. Experimental, DFT calculations and MC simulations concept of novel quinazolinone derivatives as corrosion inhibitor for mild steel in 1.0 M HCl medium. J Mol Liq. 2020;312:113413.
8. Galai M, et al. Chemically functionalized of 8-hydroxyquinoline derivatives as efficient corrosion inhibition for steel in 1.0 M HCl solution: Experimental and theoretical studies. Surf Interfaces. 2020;21:100695.
9. Ouakki M, et al. Investigation of imidazole derivatives as corrosion inhibitors for mild steel in sulfuric acidic environment: Experimental and theoretical studies. Ionics. 2020;26:5251-5272.